



Understanding dislocation slip in stoichiometric rocksalt transition metal carbides and nitrides

Hang Yu^{1,*} , Mohammadreza Bahadori¹, Gregory B. Thompson², and Christopher R. Weinberger^{1,3}

¹Mechanical Engineering and Mechanics Department, Drexel University, 3141 Chestnut, Philadelphia, PA 19104, USA

²Metallurgical and Materials Engineering, The University of Alabama, Tuscaloosa, AL 35487, USA

³Department of Mechanical Engineering, Colorado State University, Fort Collins, CO 80523, USA

Received: 13 September 2016

Accepted: 28 January 2017

Published online:

9 February 2017

© Springer Science+Business Media New York 2017

ABSTRACT

The slip systems for B1 MX compounds (M=Ti, Zr, Hf, V, Nb, Ta and X=C, N) have been studied extensively both experimentally and computationally as they influence the materials mechanical behavior at both high and low temperatures. Despite many investigations, the differences in observed slip systems, either {111} or {110}, in these materials remain an open question. In this paper, the factors that may determine the slip preference of these compounds have been studied based on the results from first principle calculations. The generalized stacking fault surfaces for all of the materials were computed and used to provide a more comprehensive understanding of slip plane choices. Through analysis of this data, it is found that among different indicators of slip, the normalized splitting width and the intrinsic stacking fault energy are the most useful indicators of the choice of slip planes in these materials. In addition, these indicators of slip are controlled by the structural energy differences between the B1 and tungsten carbides structures, which are correlated well with the number of valence electrons.

Introduction

Ultrahigh temperature ceramics (UHTCs) are a class of materials that exhibit melting temperatures above 3000 K, which is limited to roughly 30 known compounds [1, 2] and are of particular interest in high-temperature applications. A major subclass of UHTCs are the rocksalt (B1)-structured transition metal carbides and nitrides (TMC/Ns). These materials have applications including use as structural components, thermal barrier coatings and cutting tools due to their thermal stability and high hardness.

Similar to most other ceramics, TMC/Ns are hard and brittle at room temperature. However, above roughly 30% of their melting temperature, T_m , they undergo a classic brittle to ductile transition [3] and exhibit classic ductility. Numerous investigation have been undertaken to understand the fundamental reasons behind the transition between brittle behavior at low temperatures and ductile behavior at high temperatures [3].

The high-temperature ductility of the TMC/Ns was attributed to the thermal activation of a sufficient number of high-mobility slip systems. The von Mises

Address correspondence to E-mail: hy335@drexel.edu

criterion for general plastic deformation [4] states that a sufficient number of mobile slip systems must be activated for a material to behave in a ductile manner. Hollax et al. [5] have suggested that the von Mises criterion as applied to the transition metal carbides works well at high temperatures because all of the group IVB and VB carbides slip on $\{111\}$ planes, among others, which more than satisfy this criterion.

However, at low temperatures (e.g., room temperature) where these materials are classically brittle, many of the TMC/Ns exhibit different slip systems. All of these slip systems involve the $\langle 110 \rangle$ direction, but differ in the operative slip plane, which primarily slip on the $\{111\}$ or $\{110\}$ with the occasional report of $\{100\}$. This is in spite of the fact that these materials have the same structure (B1) as well as similar types of bonding. Two major experimental methods have been widely used to identify the slip system in these materials. The first method is hardness anisotropy (HA) which measures the variation of indentation hardness with respect to the angle of Knoop indenter on a specific surface (usually the $\{100\}$ and $\langle 100 \rangle$ in a cubic crystal) [6]. The variation of the hardness with angle allows one to infer which slip systems are active. The other method uses transmission electron microscopy (TEM) to directly observe the slip systems in the crystal through dynamical imaging. The advantage of the TEM is that these observations are direct and do not rely on theoretical models to infer slip systems. However, the use of TEM can be tedious and cannot eliminate certain slip systems since one can always argue that the slip systems are actually present but were simply not observed in the particular area of investigation. It is interesting to note, however, that HA measurements have been largely verified by direct TEM evidence.

For the transition metal carbides, the group IVB carbides, TiC [7], ZrC [8] and HfC [9] have been found to predominantly slip on the $\{110\}$ planes at room temperature from HA. ZrC has also been found to slip on the $\{100\}$ and $\{111\}$ planes, depending on the stoichiometry and loading conditions [10], with the dominant slip system being the standard $\langle 110 \rangle \{110\}$ from observations in TEM. TEM evidence has also demonstrated that both TiC [11, 12] and HfC [9] slip only on the $\{110\}$ planes. For the group VB carbides, the non-stoichiometric B1 structure VC_{0.84} has been found to slip on both the $\{111\}$ and $\{110\}$ planes using HA [13] with no TEM

investigations completed to date. It is worth noting that VC does not form the normal rocksalt structure, but is always significantly sub-stoichiometric with the aforementioned experiments occurring at approximately VC_{0.84}. This is a result of the lack of thermodynamic stability of stoichiometric VC, which is the only known group VB transition metal carbide to exhibit this behavior. HA measurements in NbC have also shown slip to occur on both the $\{111\}$ and $\{110\}$ planes; however, TEM evidence has only reported $\{111\}$ slip [14]. Finally, TaC has been shown to slip on the $\{111\}$ planes using both HA [9] as well as direct TEM observations [15].

For the transition metal nitrides, TiN has been identified to slip on the $\{110\}$ [16, 17], $\{100\}$ [18] or $\{111\}$ [18] planes in thin films using the TEM. However, bulk TiN has been found to slip on $\{111\}$ [19] by HA. TEM work in ZrN has shown slip on both the $\{111\}$ and $\{110\}$ planes [20]. Finally, recent experiments on the deformation of HfN at low temperatures have conclusively shown slip on the $\{111\}$ planes in this material using direct TEM observations [21]. For the group VB nitrides, the authors are unaware of any experimental investigations of slip in these materials. However, this may be in large part because the B1 structure is often listed as a high-temperature phase with reports of a low-temperature B1 structures existing as thin films. This structure is likely locked in due to the high temperatures associated with processing inherent to physical vapor deposition. The small-scale nature of these materials perhaps as inhibited the use of mechanical deformation studies on this B1 class of nitrides.

These experimental studies demonstrate that the choice of slip systems of the TMC/Ns at temperatures below the brittle to ductile transition (e.g., room temperature) is indeed complex. In order to understand the factors that control the differences in slip system choices of the TMC/Ns, several theoretical studies have investigated this phenomenon [9, 15, 22–24]. Hollox and Rowcliffe [9] used a hard sphere model, based on the ionic radii of the constituent elements, and the principle of minimum uplift to compute the preferred slip planes. This model favors $\{111\}$ slip in all of the carbides and fails to accurately capture even the trends. More recent work by Zhang et al. [22] investigated the different plastic behavior between TiN and TiC as a case study for general TiC/Ns using density functional theory (DFT). They suggested that different stacking fault

Table 1 Number of electrons explicitly modeled in the DFT simulations for each element

Element	Electrons modeled	Element	Electrons modeled	Element	Electrons modeled
Ti	$3d^24s^2$	V	$3d^34s^2$	C	$2s^22p^2$
Zr	$4d^25s^2$	Nb	$4p^64d^45s^1$	N	$2s^22p^3$
Hf	$5d^26s^2$	Ta	$5d^36s^2$		

energy and bonding strength is the key to TMC/Ns' plastic behavior, although they overlooked the importance contribution that intrinsic stacking fault (ISF) can play in plastic behavior. De Leon et al. [15] also used density functional theory to compute stacking fault energies in TaC and HfC to understand the experimentally observed differences in slip planes. The authors pinpointed the existence of the ISF in VB carbides and being a key factor in determining the slip planes and demonstrated, using a Peierls-Nabarro (PN) model, that this has a dramatic effect on the dislocation splitting width and thus slip resistance on the {111} planes. They further postulated that the existence of the ISF was a result of the valence electron charge (VEC). Thus, the VEC can potentially control the slip plane choices in these materials. The VEC has previously been regarded as a key parameter that controls the hardness and stiffness of TMC/Ns and their alloys [23–25].

In this paper, we seek to extend the work of De Leon et al. [15] to understand the slip in all of the B1-structured TMC/Ns at low temperatures. Notably, we will determine which of the group IVB and VB carbides and nitrides have ISFs and determine if this simple marker correlates well with the observation of slip on {111} planes. Since many materials exhibit several slip systems, alternative criteria, such as dislocation splitting widths on the {111} planes, may provide a better indicator of slip plane preferences. In addition, we will investigate how well the VEC model is able to predict the formation of an ISF by examining correlations between the VEC and the value of ISF. This will provide important information regarding the validity of the VEC as a parameter controlling the ISF because the VB carbides and IVB nitrides have the same VEC. This study will also extend our knowledge of the stacking fault energy curves to all of these materials including the VB nitrides, which have not been studied to date. A thorough investigation of the stacking fault energies as they relate to other structural parameters will further provide insight into what other physical

properties of the materials may control stacking fault energies and, eventually, the slip planes of these materials.

Methods

Density functional theory calculations

In order to study the slip systems in B1 TMC/Ns, we calculated the generalized stacking fault (GSF) energy surfaces using electronic structure density functional theory. These calculations were done using the Vienna *ab-initio* Simulation Package [26–29] (VASP) using a plane wave basis. The projector augmented wave [30, 31] (PAW) pseudopotentials were used in all calculations, and the exchange-correlation energies were evaluated using the formulations of Perdew–Burke–Ernzerhoff (PBE) within the generalized gradient approximation (GGA) [32]. The electrons explicitly involved in the calculations are listed in Table 1. The cutoff energy for the plane wave was 600 eV and found to be sufficient to converge the total energies. Structural relaxations were performed using the conjugate gradient method for ion relaxation and the criteria used for termination of the ionic relaxation was set to $1e-4$ eV. K-space integration was performed using a Gamma-centered scheme where the number of integration points were kept at $9 \times 9 \times 1$ for structural relaxation and $15 \times 15 \times 1$ for density of states (DOS) calculations.

GSF calculation

The calculation of all of the GSF surfaces used large supercells based on the extension of the B1 structure. The lattice constants, a_0 , of the B1 structures for all of the compounds were computed via conjugate gradient minimization in small periodic cells, and these lattice parameters were used as the basis for the supercells used in the computation of GSF surfaces. The structure used in computation of the GSF

surfaces for the $\{111\}$ plane was described using a trigonal basis $\mathbf{a}, \mathbf{b}, \mathbf{c}$ where the bases vectors are aligned with the $[\bar{1}10], [10\bar{1}]$ and $[111]$ directions relative to the B1 structure. For the $\{110\}$ GSF surface, an orthorhombic setting was used where the $\mathbf{a}, \mathbf{b}, \mathbf{c}$ vectors are set to the $[110], [001]$ and $[\bar{1}\bar{1}0]$ in the B1 structure. All of the GSF supercells contain 24 layers of atoms normal to the slip plane, and a vacuum gap was used to create free surfaces and break the periodicity in the z -direction. The 15 Å gap was determined from DFT calculations of the separation of a $\{111\}$ plane in TaC where the gap was increased from 0 to 20 Å. At 15 Å, the fluctuation in the as-computed GSF energy is 2.8 mJ/m² for gaps ranging from 10 to 20 Å, demonstrating that the change in gap is insignificant compared to the energies reported below. The fault was created in between the middle metal–nonmetal planes. The GSF energy surfaces are then computed as the structural energy differences between faulted and un-faulted structures.

Results

GSF surfaces and curves

The GSF surfaces for the $\{111\}$ planes in all of the group IVB and VB carbides and nitrides were computed using DFT. An example of such a GSF surface is shown below in Fig. 1 for the case of niobium carbide. This GSF surface is very reminiscent of what a GSF surface would look like in a face-centered-cubic (FCC) metal with the existence of a local minimum near at the $\frac{1}{6}\langle 112 \rangle$ point. At this point, the symmetry of the $\{111\}$ plane dictates that this point must be a local extremum (minimum, maximum or saddle point) and the local energy minimum is associated with a stacking fault in this material. In the case of the B1 structure, the stacking sequence transforms from $\dots A\gamma B\alpha C\beta A\gamma B\alpha C\beta \dots$ of the perfect crystal to the stacking sequence of the ISF, which is $\dots A\gamma B\alpha C\beta | C\beta A\gamma B\alpha \dots$, as illustrated in Fig. 2, where “|” indicates the position of faulted plane. Further along the $\langle 112 \rangle$ path, the curve reaches a global maximum which corresponds to the stacking of a metal atom directly above the nonmetal atom, i.e., $\dots A\gamma B\alpha C\beta | B\alpha C\beta A\gamma \dots$ which is the most unfavorable stacking position.

Slip on the $\{111\}$ planes should occur via a perfect dislocation with Burgers vector $\frac{a}{2}\langle 110 \rangle$. However, the

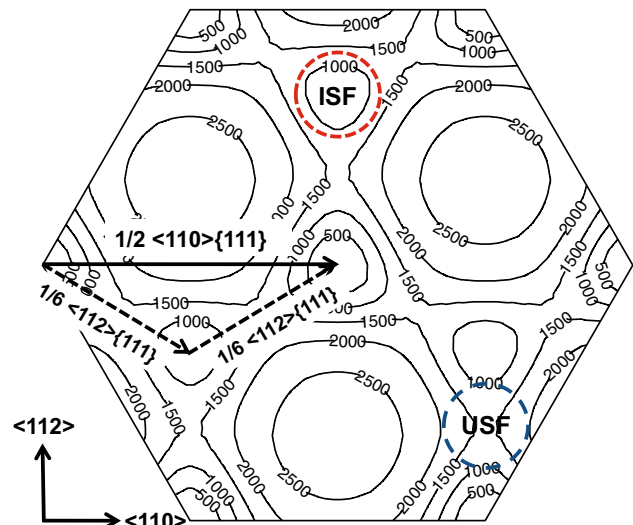


Figure 1 A contour plot of the GSF surface for NbC on the $\{111\}$ plane, in mJ/m². The arrows highlight the perfect dislocation (solid line) and how the perfect dislocation may separate into two partial dislocations (dashed line) as slip proceeds through the ISF configuration (circled by the red short dashed line) and the energy barrier it has to overcome, which is the unstable stacking fault (USF) (circled by the blue long dashed line).

existence of an ISF makes it possible for the perfect dislocation to split into two Shockley partial dislocations with Burgers vectors in the $\langle 112 \rangle$ directions as shown in Fig. 1. As noted previously, De Leon et al. [15] pointed out that in the case of the IVB carbides, such a local minimum, e.g., the ISF, does not exist which would favor slip on the $\{110\}$ planes. However, the total GSF surface was not computed nor were the GSF curves for the group IVB and VB nitrides, which also form the B1 structure.

Figure 3a1–d1 shows representative GSF surfaces for each of the group IVB carbides, VB carbides, IVB nitrides and VB nitrides, respectively, with the GSF curves for the $\langle 110 \rangle$ and $\langle 112 \rangle$ directions on the $\{111\}$ planes as well as the $\langle 110 \rangle$ direction on the $\{110\}$ planes. A general feature that is consistent between all of the carbides and nitrides studied here is that the GSF curves for the $\langle 110 \rangle$ directions on the $\{110\}$ planes are lower than those on the $\{111\}$ planes. This feature would suggest, in the absence of the potential for slip via partial dislocations, that the $\{110\}$ planes would be favored as the slip planes, which happen to be the dominant slip planes in ionic bonded B1-structured crystals like NaCl. However, the rest of the GSF surfaces differ between the transition metal

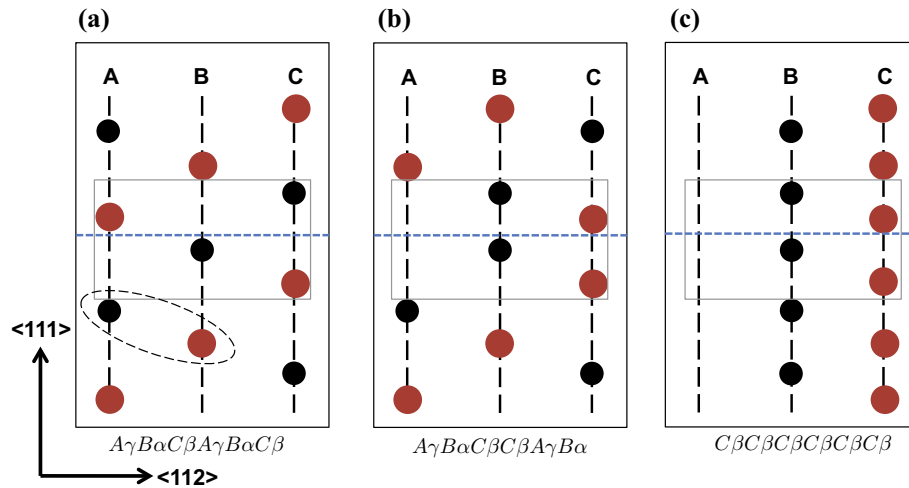


Figure 2 An illustration of the stacking sequence of the **a** rocksalt structure **b** the rocksalt structure with a stacking fault and **c** the tungsten carbides structure. The *red balls* represent metal atoms and *black balls* represent nonmetal atoms. The *blue dashed line* denotes the shear plane, which is always between metal and nonmetal atoms. The *thin box* highlights the 4 atoms closest to the

shear plane. The *black dashed line* encloses the second nearest neighbor metal and nonmetal atoms away from the shear plane. Using this as a guide, one can see the similarity of local stacking sequences of the faulted B1 structure and the tungsten carbide structure.

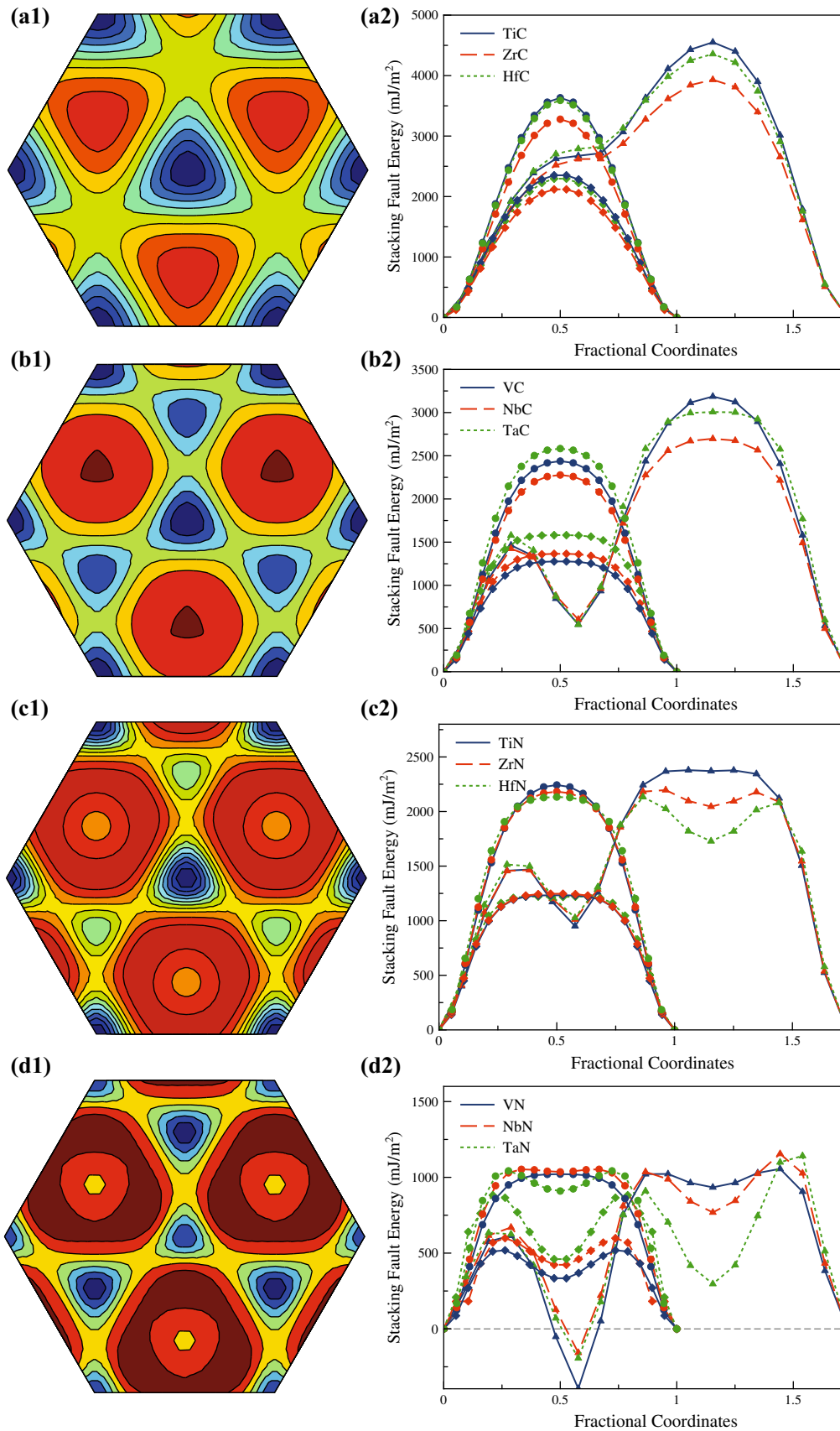
group as well as nonmetal atoms, and these features will be discussed in the following paragraphs.

In the group IVB carbides, shown in Fig. 3a1, a2, the GSF surface lacks a local minimum, or ISF, as pointed out by De Leon *et al* [15]. As dictated by symmetry, the ISF must be an extremum; however, in this material class the extremum becomes a point of inflection, rather than a classic saddle point or a local minimum or maximum. In fact, the shape is commonly referred to as a “monkey saddle” [33]. The existence of the point of inflection is clear since all directions about the point where the ISF would normally be located, the local second derivative is zero. The existence of this inflection eliminates the USF, which is the maximum between the global minimum (un-faulted structure) and the ISF and should occur at $\frac{a}{12} \langle 112 \rangle$ if one relies solely on a simple hard sphere model. Since the GSF surface must obey the threefold symmetry of the $\langle 111 \rangle$ zone, the maximum and minimum take on triangular shapes in the plane. This may also be an indicator of a stronger, directional bonds between the atoms.

The group VB carbides were discussed above in the case of NbC and the other group VB carbides have similar GSF surfaces and curves, as shown in Fig. 3b1, b2. All of the energies are lower than the group IVB carbides, and the presence of the ISF and

the associated local minima is clear. A local maxima occurs in between the global and local minima, known as the USF, at around the $\frac{a}{12} \langle 112 \rangle$ point. In this case, the shape of the GSF surface changes. The ISF and global minimum (un-faulted structure) appear both triangular in nature and thus split in the area of the global maximum into what appears to be a more hexagonal or circular shape.

In the case of the group IVB nitrides, Fig. 3c1, c2, the GSF surface still possess a local minimum at the ISF position and a USF at roughly the same point as the VB carbides. This results in a curve that is similar shape to the VB carbides. The USF in both classes of materials are very similar; however, the IVB nitrides have a higher ISF compared to VB carbides. Thus, the global maximum appears to have a hexagonal shape that is more distorted, i.e., it appears less of a regular hexagon than the VB carbides. The other interesting phenomenon that occurs in the group IVB nitrides is the emergence of another local minimum at the $\frac{2a}{6} \langle 112 \rangle$ position. In the carbides, as well as closed packed metals, this is the position of a global maximum. The local minimum is very shallow for TiN, but its depth increases with increasing atomic number is well established in HfN. This new local minimum indicates reduced repulsion when the metal atom is sitting right above the nonmetal atom, i.e., Az



◀**Figure 3 a1–d1** Representative GSF surfaces on the $\{111\}$ planes for the four representative TMC/Ns. **a2–d2** The GSF curves for each of the TMC/N materials plotted in fractional coordinates. The coordinate is normalized by the length of the perfect Burgers vector ($a_0/\sqrt{2}$) as shown in Fig. 1. The GSF curve for the $\langle 110 \rangle \{110\}$ is represented by *diamonds*, the $\langle 110 \rangle \{111\}$ by *dots*, and the $\langle 112 \rangle \{111\}$ by *triangles*. Note that the directions of the $\langle 110 \rangle \{111\}$ and $\langle 112 \rangle \{111\}$ GSF curves are given in Fig. 1.

stacking, compared to the slightly shifted stacking. However, we expect this to have no effect on slip, despite its emergence in the nitrides.

For the group VB nitrides, Fig. 3d1, d2, the ISF configuration appears to be more stable than the B1 structure. This suggests that the B1 structure is not the lowest energy structure predicted by DFT at 0K. In both NbN and TaN, the hexagonal epsilon phase is usually predicted to be more stable at low temperatures. However, the B1 structure is often reported as a high-temperature polymorph for these materials and can be fabricated as thin films and stabilized at room temperature [34]. Thus, the GSF surfaces are very similar to the group IVB nitrides and the locations of the global and local minima are switched. The other interesting feature is the $\frac{2a}{6} \langle 112 \rangle$ point, which is a local minimum even lower than the IVB nitrides. However, this configuration is surrounded by relatively high local maxima which likely would prevent slip through this position. Thus, the new local minima likely have no influence on slip.

Determining the predictors of low-temperature slip

The hypothesis put forth by De Leon et al. [15] states that $\{111\}$ slip in the B1 TMC/Ns is controlled by the existence of an ISF in the material. They also pointed out that the presence of an ISF coincided with an additional valence electron in the B1 structure and thus suggested that the presence of $\{111\}$ slip in these materials, i.e., a more ductile behavior, can be linked to a VEC argument. The inclusion of the B1 structured transition metal nitrides will allow us to test this hypothesis, especially since the IVB nitrides and VB carbides have the same VEC, as well as search for other indicators of $\{111\}$ slip in these materials. In addition, such a study will allow us to better identify the underlying causes that transition the ISF from a local minimum to an inflection point.

The first idea we will present is the hard sphere model. This model is based on geometric arguments centered on the radius ratio of the nonmetal atom to the metal atom, r/R . The idea put forth by Van Der Walt and Sole [35], and applied to the carbides by Rowcliffe and Hollox [9], suggests that $\{110\}$ slip occurs for $r/R < 0.414$, $\{111\}$ slip for $0.414 < r/R < 0.633$ and $\{100\}$ slip for $r/R > 0.732$. This model also predicts that dislocations will split on the $\{111\}$ plane for $r/R > 0.732$. Hollox and Rowcliffe suggested that while the model strictly predicted $\{111\}$ slip for all the compounds, there was still a tendency for materials with smaller radius ratios to slip on the $\{110\}$ planes. However, such work is based on the use of ionic radii and the TMC/Ns are not ionic solids. This raises the question of whether or not DFT can provide better input to this model using computationally derived atomic sizes. This can be approached using Bader charge analysis [36], which can be used to estimate atomic volume and hence atomic radius ratios. Our results from DFT and Bader charge analysis give the radius ratios of near 1 for all the compounds. Obviously, the combination of the DFT volume analysis and the hard sphere model are incapable of differentiating either the existence of stacking faults, which could be potentially atomic size dependent, or the choice of slip planes. The Bader derived atomic ratios are too uniform to be any indicator of slip planes choice or stacking fault energies. Thus bonding is key in determining slip as expected [15, 22, 37].

The GSF curves along the $\langle 110 \rangle$ directions on the $\{111\}$ and $\{110\}$ planes do not provide a good indicator of the preference of slip planes either. However, it does provide evidence that perfect slip on the $\{111\}$ plane is unlikely to happen. As shown in Fig. 3a2–d2, the energy barrier of $\langle 110 \rangle \{111\}$ is always higher than of $\langle 110 \rangle \{110\}$. An alternative measure of the resistance to slip is the maximum of the stress required to move along this path, which is a measure of the ideal shear strength. These shear stresses, which we have denoted as τ , have been computed and are listed in Table 2. The general trend is $\tau_{\langle 110 \rangle \{110\}} < \tau_{\langle 112 \rangle \{111\}} < \tau_{\langle 110 \rangle \{111\}}$ with exceptions of group VB nitrides. However, since the VB nitrides do not form the B1 structure at room temperature, this deviation is not surprising. The ideal shear stress results also suggest that the $\langle 110 \rangle \{111\}$ is unfavorable compared to the other two slip systems. This evidence suggests that

Table 2 Structural and material parameters calculated from DFT simulations as well as derived parameters that may indicate these materials' choice of slip planes

	TiC	ZrC	HfC	VC	NbC	TaC	TiN	ZrN	HfN	VN	NbN	TaN
a_0 (Å)	4.34	4.73	4.65	4.16	4.50	4.48	4.25	4.61	4.54	4.13	4.45	4.44
VEC	8	8	8	9	9	9	9	9	9	10	10	10
Δe^-	1.44	1.67	1.73	1.32	1.70	1.70	1.55	1.67	1.71	1.54	1.66	1.67
ΔE_{SL}	-0.04	-0.15	-0.10	0.44	0.45	0.51	0.20	0.16	0.22	-0.22	-0.32	-0.51
ISF (J/m ²)	2.67	2.62	2.79	0.55	0.61	0.55	0.95	1.01	1.03	-0.39	-0.16	-0.19
USF (J/m ²)	1.93	1.78	1.92	1.46	1.42	1.58	1.46	1.46	1.52	0.62	0.67	0.63
ISF/USF	1.39	1.47	1.45	0.37	0.42	0.35	0.65	0.70	0.68	-0.64	-0.23	-0.31
c_{11} (GPa)	530	474	525	652	562	685	613	630	659	582	679	738
c_{12} (GPa)	130	115	118	141	166	163	134	103	107	185	115	130
c_{44} (GPa)	163	144	164	188	149	158	169	124	128	92	70	35
$d_{0^\circ}^*$	0.34	0.33	0.35	1.94	1.42	1.89	1.04	0.96	0.97	-	-	-
$d_{30^\circ}^*$	0.39	0.39	0.41	2.23	1.71	2.27	1.21	1.16	1.18	-	-	-
$d_{60^\circ}^*$	0.49	0.49	0.50	2.76	2.24	2.85	1.50	1.36	1.37	-	-	-
$d_{90^\circ}^*$	0.54	0.54	0.55	3.04	2.52	3.18	1.65	1.51	1.52	-	-	-
Anisotropy factor	0.82	0.80	0.81	0.74	0.75	0.61	0.71	0.47	0.46	0.46	0.25	0.11
r/R	1.13	1.05	1.04	1.08	1.00	1.00	1.10	1.01	1.00	1.08	0.97	0.96
$\tau_{(112)\{111\}}$ (GPa)	28.0	23.6	25.7	24.4	22.3	25.3	23.7	22.2	23.9	12.8	12.2	12.5
$\tau_{(110)\{111\}}$ (GPa)	37.7	31.1	34.5	32.2	28.6	33.7	30.4	28.9	31.2	18.9	19.3	21.9
$\tau_{(110)\{110\}}$ (GPa)	26.4	21.4	23.3	20.5	20.5	24.6	21.2	20.2	21.6	12.5	29.6	29.2

The reported ISF and USF values were taken from the expected geometric points, rather than using the local minimum and maximum values, which was done because the IVB carbides have neither a local maximum nor minimum. The normalized splitting width, $d^* = d/a_0$, was calculated for different angles between dislocation line direction and Burgers vector, which is denoted in the subscript. The maximum stress values τ were computed from the slope of the GSF curves in the indicated directions. The charge transfer Δe^- for B1 TMC/Ns was computed using Bader charge analysis. ΔE_{SL} represents the intensity of the nonlocal effect, which quantifies the deviation in Fig. 4c, units in eV/atom on the plane

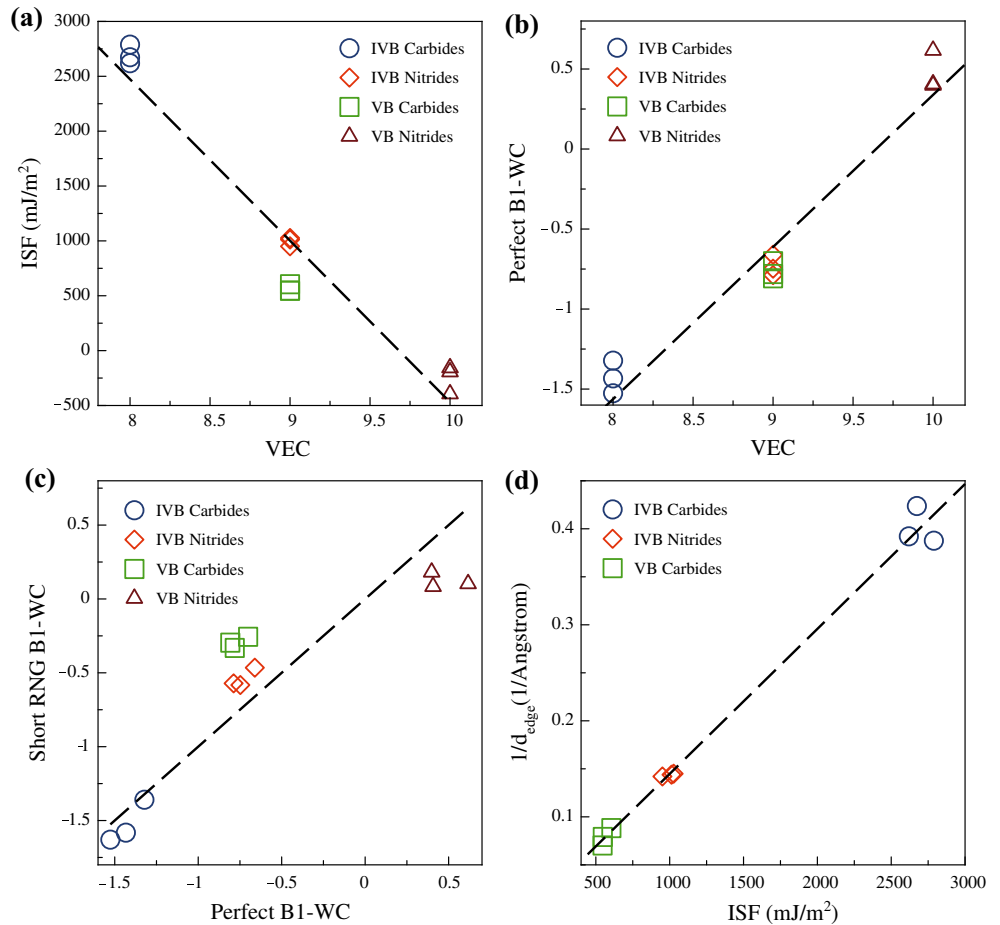
the only possible mechanism to slip on $\{111\}$ plane is through partial dislocations. We note that the ratio of the ISF to USF does provide a trend that the higher this ratio, the less likely the material is to slip on $\{111\}$ planes. Please note that in our evaluation of the USF, we use a strict geometric definition and evaluate it at the $a/12\langle 112 \rangle$ position. However, the USF (see Table 2) varies little between the materials (if we omit the VB nitrides), which indicates it is indeed the value of the ISF that really controls the slip planes. Thus, it is very important to consider the ISF value and what controls its value.

The VEC parameter has been used previously to describe property variations like hardness [25, 38–40] in these materials and may correlate with the ISF [15]. To test this idea, we plot the VEC versus ISF value in Fig. 4a. To make this comparison concrete, we have taken the values for the ISF to occur exactly at the $\frac{a}{6}\langle 112 \rangle$ point on the GSF surfaces which is necessary to include the IVB carbides. For the VEC, it is common in these materials to take it as the number of

valence electrons, which are the 2s and 2p electrons in the nonmetal atoms and the outermost s and d shells of the transition metal atoms, and report the number per formula unit. A simple correlation coefficient analysis, which tests for linear correlation, results in a value of -0.89. This suggests a relatively strong correlation between the VEC and the ISF value. On the other hand, the charge transfer Δe^- of B1 TMC/Ns was also tested and presented in Table 2. However, this value does not predict the slip system well. For instance, the Δe^- for HfC and TaC is very close with difference less than 2%, while HfC is confirmed to slip on $\{110\}$ plane and TaC slip on $\{111\}$ plane and have large differences in stacking fault energies.

The correlation of the VEC and ISF values does not, however, provide a deeper understanding into the causes of the change of ISF with VEC. Furthermore, it cannot explain why the ISF becomes negative in the VB nitrides or the differences between IVB nitrides and VB carbides. To provide a better structural

Figure 4 Selected correlations between computed parameters in the B1 TMC/N. **a** The ISF value plotted as a function of the VEC. **b** The structural energy differences between the perfect tungsten carbide and B1 structures as a function of the VEC, the units of energy difference is eV/atom. **c** The relationship between the perfect B1 and WC structural energy differences versus the short range structural energy differences, units in eV/atom on the plane. **d** The inverse of edge dislocation splitting width plotted as a function of the stacking fault energy. The group VB nitrides are not included in the plot since they would have infinite dislocation splitting width due to negative ISF value.



understanding, we examine the local stacking sequence of the ISF in these materials, which is: $\dots A\gamma B\alpha C\beta \mid C\beta A\gamma B\alpha \dots$. A close inspection of the stacking sequence shows that the fault itself centers around a stacking sequence of $\dots C\beta \mid C\beta \dots$, which locally has the tungsten carbide (WC) structure. This may indicate that the local bonding in the ISF is similar to the WC structure and the value of the ISF may be controlled by the associated structural energy differences. To test this, we computed the structural energy differences, per atom, of the B1 and WC structures for all 12 of the compounds studied here as shown in Fig. 4b. From this plot, it is clear that the B1 structure is favored over the WC structure for all of the carbides and the IVB nitrides, all of which have positive stacking fault energies. For the VB nitrides, the structural energy difference is negative which agrees with the negative stacking fault energies. The correlation coefficient computed is high, 0.82, between the structural energy differences and VEC. It is interesting to note that we see little difference

between the IVB nitrides and VB carbides. This suggests that differences in the computed ISF values are not directly related to the structural energy differences between the B1 and WC structures.

Since the B1 and WC structural energy differences are similar among the IVB nitrides and VB carbides, this suggests the difference in stacking fault energies between these two groups of compounds is related to bonding that extends beyond the first 4 layers of atoms around the slip plane (see Fig. 2). In order to test this idea, the local density of states (LDOS) and partial density of states (PDOS) of the metal and nonmetal atom that are second nearest to the shear plane have been calculated and plotted in Fig. 5. By comparing the LDOS/PDOS before and after shearing, the effect of shearing on these second nearest atoms can be determined. For TiC, the change in all types of bond is minimal, suggesting that these atoms are minimally influenced by shearing in the crystal. For TaC, the most discernible change takes place around -5 eV which shows strong evidence of p-d

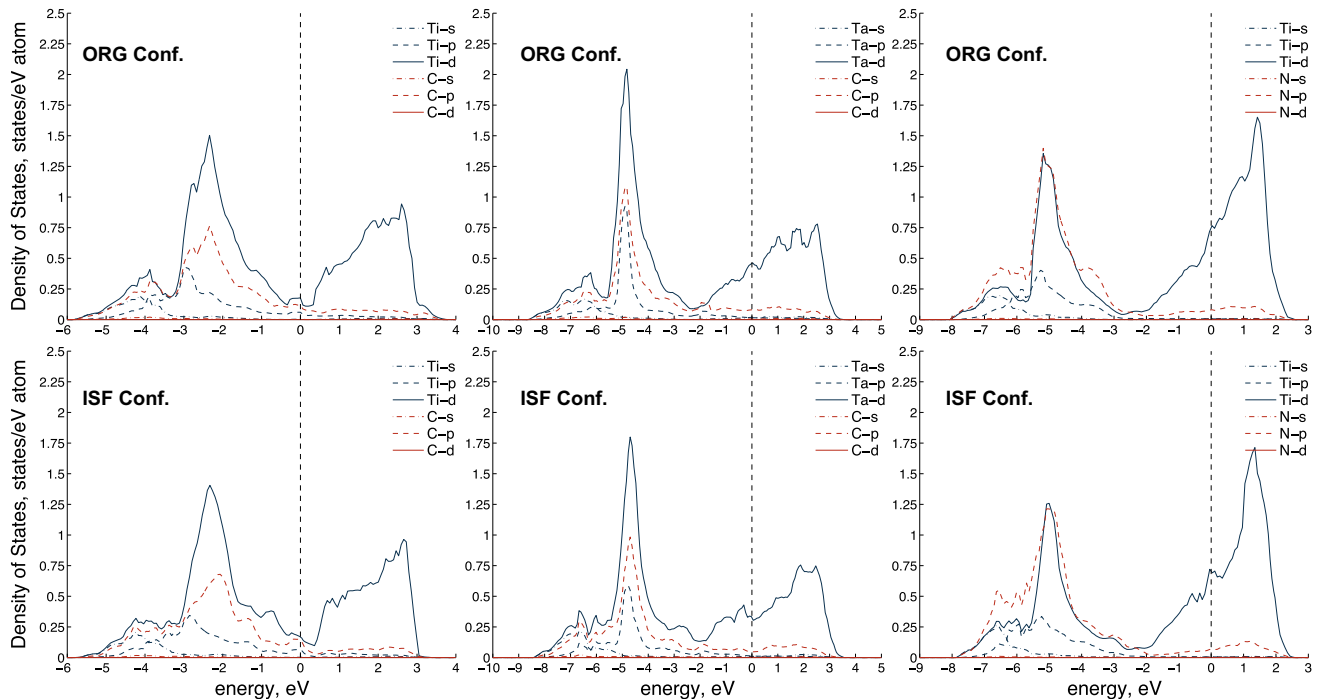


Figure 5 LDOS/PDOS computed at the metal and nonmetal atoms shown in Fig. 2 in the *dashed ellipse*. These atoms are closest to, but not directly involved in, the bonding around the slip

bonding. The decrease in the DOS of Ta-*d* and Ta-*p* is obvious, as opposed to the C-*p*, which do not change. For TaC, there is also a change in DOS around the Fermi level, which is controlled by the *dd* metal bonds in the material. For TiN, the change is not as noticeable as TaC, but larger than TiC. This provides some insight into the electronic structure origins of the role nonlocal contributions to the stacking fault energies, but fails to provide quantitative evaluation of this effect.

To investigate this quantitatively, we plot the perfect B1-WC structural energies versus those for a short range structural energy differences in Fig. 4c. The short range structural difference differs from the ISF in that it represents the energy difference per atom on the plane rather than per unit area. The short range WC has the stacking sequence of the ISF, while the short range B1 has the original stacking sequence before shearing. The straight line with slope of one plotted here indicates a perfect dependence of the short range energy difference on the perfect B1-WC structural energy difference and points lying on this line indicate the stacking fault energies are completely determined by the four atoms closest to the slip plane. It is clear that the group VB carbides

plane and thus potentially contribute to higher-order effects in the stacking fault energies.

deviate from this ideal relationship more than group IVB nitrides, with the energy deviation from this straight line provided in Table 2. This deviation, ΔE_{SL} , is computed as the difference between the short range energy B1-WC minus the perfect B1-WC energy differences. This is indicative of higher-order interactions being important in determining stacking fault energies. We have noted in previous work [41] that the stacking fault phases in tantalum carbides have higher-order interactions that are necessary to describe the faults; this may be a universal characteristic in the bonding of the group VB carbides. This helps explain why VB carbides and IVB nitrides have significant differences in ISF energies, Table 2, while having the same VEC. Although this nonlocal effect can also be found in group VB nitrides, it is not quite as strong.

This finding provides a detailed understanding of what controls the values of the ISFs; however, we still need to provide an indicator of {111} slip that is better than the VEC. To provide an improved discussion on the stabilization of dislocations on the {111} planes, we appeal to the idea of dislocation splitting widths. This was pointed out to be important [15] in determining the slip planes in TaC and

HfC, but was not developed for other carbides or nitrides nor was it used as a clear indicator of slip plane preference. While the PN model used previously is robust, it is not expedient and thus we investigate classical models of the splitting width as given in Hirth and Lothe [42] for anisotropic cubic materials. The computed dislocation splitting widths for dislocations with varying line directions are shown in Table 2 and demonstrate that the splitting widths are greatest in the VB carbides and smallest in the IVB carbides.

Figure 4d shows the inverse of the splitting width of edge dislocation with respect to the stacking fault energies, giving the expected linear trend as the variation of elastic constants is minimal compared to the stacking fault energies. This linear relationship can be written as $1/d = \beta_0 + \beta_1 \times ISF$, where β_0 and β_1 are related to the dislocation line direction. The two constants for the different dislocation line directions have been provided in Table 3. The group VB nitrides are excluded because the splitting width should be infinite owing to the negative stacking fault energies, and this issue will be discussed in detail later.

The dislocation splitting width becomes a critical parameter in determining slip planes because the smaller the splitting width, the larger the stress is required to move the dislocations. As the splitting width is reduced to zero, the dislocations no longer follow the $\langle 112 \rangle$ path and rather form perfect $\langle 110 \rangle$, which are energetically more favored to move on the $\{110\}$ plane by our GSF calculations. Therefore, the larger the splitting width, the more likely the material is to slip on the $\{111\}$ planes. Another advantage of using the dislocation splitting width as an indicator of the preference to the slip planes is that the parameter is continuous, as opposed to the existence of an ISF as suggested in [15], which has the potential to allow for a continuous transition from $\{111\}$ to $\{110\}$ slip. This feature is probably desirable because we note that in experiments, in some materials both

$\{110\}$ and $\{111\}$ slip are observed and that additional factors, such as load type, might influence the choice of slip planes. However, we note that dislocation splitting widths are not scale independent and thus we choose to normalize by the lattice constant, i.e., $d^* = d/a_0$, so that this normalized splitting width can be used as an indicator of the materials preference to $\{111\}$ slip at low temperatures.

High-temperature approximation in group VB nitrides

As previously mentioned, the bulk group VB nitrides are found to form other structures at low temperature and thermodynamically form the B1 structure at higher temperatures. Experimental results suggest that VN_x forms the B1 structure above 1000K [43], NbN above 1200K [44] and TaN forms rocksalt structure at near 2000K [45]. The negative ISF energy and direct DFT simulations have shown that the tungsten carbide structure is more stable than the B1 structure at 0K. Thus, if the B1 structure were stabilized at room temperature, which has been reported experimentally, then we would expect slip to be favorable on the $\{111\}$ planes but we expect that the deformation would be through faults converting the less favorable B1 structure to the more favorable tungsten carbide structure.

This apparent preference to $\{111\}$ slip agrees with the simple VEC argument, nevertheless it does not provide enough insight to understand what would happen at higher temperatures where the B1 structure is stable. Recent work [46, 47] has suggested that it is insightful to look at the properties of the lattice as it expands to approximate crystal properties at elevated temperatures. We have conducted a similar study here where we have expanded the B1 lattice of NbN and computed the GSF energy curve in the $\langle 112 \rangle$ direction as shown in Fig. 6. The ISF increases as the lattice constant increases, with the ISF becoming positive around 0.012 volumetric strain and eventually the GSF curve becomes similar to the group IVB nitrides and IVB carbides. The increase in ISF, achieving positive values, indicates that lattice expansion favors the B1 structure over the tungsten carbide structure. It is also interesting to note that the $2a/6\langle 112 \rangle$ point slightly decreases as well, which indicates that lattice expansion further reduces the repulsion between the ions in that stacking sequence.

Table 3 Numerical β factors that relate the splitting width to the stacking fault energies for the cubic transition metal carbides and nitrides with positive stacking fault energies

Element	0°	30°	60°	90°
β_0	−0.00673	−0.01210	−0.00617	−0.00622
β_1	0.00024	0.00021	0.00017	0.00015

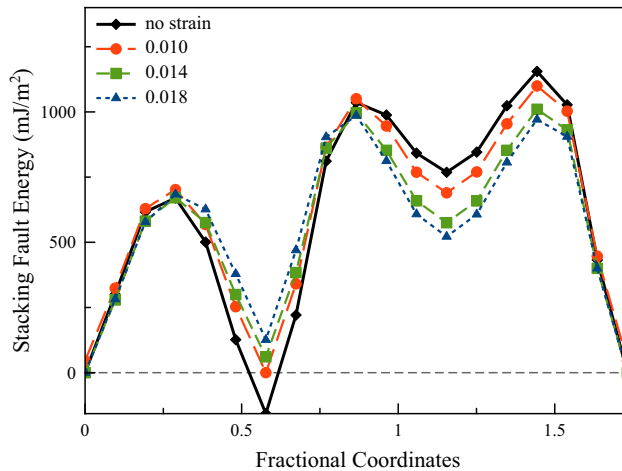


Figure 6 GSF curves of NbN along $\langle 112 \rangle\{111}$ subjected to different volumetric strains. The higher volumetric strains increase the ISF energy indicating that the rocksalt structure becomes more favorable than the tungsten carbide structure.

The observations noted above are a consequence of lattice expansion caused by the increase in temperature. It is also important to note that with an increase in temperature, the entropy also affects the free energy. Since the B1 becomes stable at higher temperatures, it can be assumed that its free energy decreases faster than the WC structure, which should cause the ISF (which is related to these structural energy differences) to rise. These trends suggest that when the group VB nitrides form the B1 structure at elevated temperatures, dislocation should dissociate on the $\{111\}$ planes and thus $\{111\}$ would be the more preferred slip plane.

Discussion

The choice of low-temperature slip planes in the B1 structure TMC/Ns is complicated. However, in this work we investigated the factors that likely contribute to the dominance of certain slip planes. To this end, we computed the GSF surfaces on the $\{111\}$ and $\{110\}$ planes for all 12 MX compounds ($M=\text{Ti, Zr, Hf, V, Nb, Ta}$ and $X=\text{C, N}$). We found that the group IVB carbides do not have an ISF or USF, but these types of faults do exist in all the other carbides and nitrides.

Using DFT-derived atomic ratios, we demonstrated that the hard sphere model is still insufficient even when using DFT-derived atomic sizes in predicting the existence of ISFs or the choice of slip planes as the radius ratios of all the compounds were similar. Rigid

slip values, computed from the slopes of the GSF curves, also provided no consistent trends as to which slip system should be preferred. However, as it is common to use the USF to ISF ratio to indicate ductility, this appears to hold true for these materials as the group IVB carbides have the largest ratio and are the most brittle in room temperature indents. Though the ratio of the USF to ISF does a good job of indicating $\{111\}$ slip, it is dominated by changes in the ISF, which varies significantly between these materials while the absolute value of the USF varies significantly less. Thus, the ISF is clearly one of the dominant factors in determining the slip planes.

The normalized splitting width, d^* is a better indicator of the general preference of the slip planes. This work shows that the most dominant factor in determining the splitting width is the ISF, with lattice constants and elastic constants playing minor roles. The splitting widths of the group IVB carbides are found to be very small, less than a single atomic spacing in the Burgers vector direction, suggesting that dislocations on $\{111\}$ plane would have very low mobility. The group IVB nitrides and VB carbides have increased splitting widths compared to the group IVB carbides, indicating a stronger preference to slip on $\{111\}$ planes. It is important to note that d^* indicates a trend, not a strict cutoff, which is reasonable because TMC/Ns such as TiN are found to slip on either $\{110\}$ or $\{111\}$ planes experimentally. It is also interesting to note that our work demonstrates that the mobility of screw dislocations should be lower than those of edge dislocations. A higher density of straight screw dislocations has been observed in low-temperature plasticity in both TaC [48] and HfN [21], providing some experimental validation. On the other hand, the VEC can be used as general guide indicating trends, which requires minimal calculation, but is not as precise as d^* especially in the case of differentiating the group VB carbides and group IVB nitrides. This difference is thought to arise from higher-order interactions that are intrinsic to the group VB carbides.

For the group VB nitrides, the negative ISF value indicates that the stable structure at 0K for those materials is not the B1 structure. The B1 structure of these compounds is most often reported as a high-temperature phase. To understand the potential role lattice expansion plays in altering the ISF of these materials, we computed the ISF as a function of lattice strain, which can mimic the effects of temperature. At

high-volumetric strains, the ISF changes from negative to a small positive value, suggesting that high-temperature slip in the group VB nitrides should be closer to that of the group VB carbides and IVB nitrides.

These results also demonstrate that the structural energy differences in these materials can influence the tendency of the material to slip on certain slip planes. The increase in the number of valence electrons makes the tungsten carbide structure more favorable, which lowers the stacking fault energy which widens dislocations on the {111} planes, reducing their resistance to slip. Ultimately, the availability of the {111} planes from slip makes these materials a little more ductile at room temperature.

Conclusion

In this paper, we have demonstrated that the normalized splitting widths of dislocations is a good parameter to determine, comparatively, the propensity of the material to slip on the {111} planes. This parameter is largely governed by the ISF value, and the normalized splitting width was chosen over the ISF since it is dimensionless and represents a mechanistic link to dislocation motion.

The ISF energy is largely controlled by the structural energy differences between the B1 and WC structures. The structural energy differences can be related to the VEC, which correctly captures the trends and can be used as a guide. However, it fails when higher-order effects are important in determining the stacking fault energies and cannot distinguish between the IVB nitrides and VB carbides. The group IVB nitrides should have a low ISF value when the B1 structure is stable. This material would prefer to slip on {111} planes when present.

The results presented here can be potentially used to guide alloying and its effects on the choice of slip planes. Alloying presumably will be able to change the VEC and hence structural energy differences, influencing the dislocation splitting widths and the choice of slip planes. Experimental efforts in this area would be useful in validating these predictions.

Acknowledgements

H. Yu and C.R. Weinberger recognize Air Force Office of Scientific Research Grant FA9550-15-1-0217, Dr. Ali Sayir Program Manager. G.B. Thompson recognize Air

Force Office of Scientific Research Grant FA9550-15-1-0095, Dr. Ali Sayir Program Manager. Work reported here was run on hardware supported by Drexel's University Research Computing Facility.

References

- [1] Wuchina E, Opila E, Opeka M, Fahrenholtz W, Talmy I (2007) UHTCs: ultra-high temperature ceramic materials for extreme environment applications. *Electrochem Soc Interface* 16:30
- [2] Fahrenholtz WG, Wuchina EJ, Lee WE, Zhou Y (2014) *Ultra-high temperature ceramics: materials for extreme environment applications*. Wiley, New York
- [3] Dieter GE, Bacon DJ (1986) *Mechanical metallurgy*, vol 3. McGraw-Hill, New York
- [4] Rv Mises (1928) *Mechanik der plastischen formänderung von kristallen*. *Z Angew Math Mech* 8:161–185
- [5] Hollox G, Smallman R (1966) Plastic behavior of titanium carbide. *J Appl Phys* 37:818–823
- [6] Hannink R, Kohlstedt D, Murray M (1972) Slip system determination in cubic carbides by hardness anisotropy. *Proc R Soc Lond A Math Phys Eng Sci* 326:409–420
- [7] Kumashiro Y, Itoh A, Kinoshita T, Sobajima M (1977) The micro-vickers hardness of TiC single crystals up to 1500°C. *J Mater Sci* 12:595–601. doi:10.1007/BF00540285
- [8] Kumashiro Y, Nagai Y, Katō H, Sakuma E, Watanabe K, Misawa S (1981) The preparation and characteristics of ZrC and TaC single crystals using an r.f. floating-zone process. *J Mater Sci* 16:2930–2933. doi:10.1007/BF00552985
- [9] Rowcliffe DJ, Hollox GE (1971) Plastic flow and fracture of tantalum carbide and hafnium carbide at low temperatures. *J Mater Sci* 6:1261–1269. doi:10.1007/BF00552039
- [10] Lee D, Haggerty J (1969) Plasticity and creep in single crystals of zirconium carbide. *J Am Ceram Soc* 52:641–647
- [11] Chien F, Ning X, Heuer A (1996) Slip systems and dislocation emission from crack tips in single crystal TiC at low temperatures. *Acta Mater* 44:2265–2283
- [12] Chatterjee D, Mendiratta M, Lipsitt H (1979) Deformation behaviour of single crystals of titanium carbide. *J Mater Sci* 14:2151–2156. doi:10.1007/BF00688420
- [13] Kumashiro Y, Sakuma E (1980) The vickers micro-hardness of non-stoichiometric niobium carbide and vanadium carbide single crystals up to 1500°C. *J Mater Sci* 15:1321–1324. doi:10.1007/BF00551827
- [14] Morgan G, Lewis M (1974) Hardness anisotropy in niobium carbide. *J Mater Sci* 9:349–358. doi:10.1007/BF00737834
- [15] De Leon N, Yu Xx YuH, Weinberger CR, Thompson GB (2015) Bonding effects on the slip differences in the B1 monocarbides. *Phys Rev Lett* 114:165502

- [16] Hultman L, Shinn M, Mirkarimi P, Barnett S (1994) Characterization of misfit dislocations in epitaxial (001)-oriented TiN, NbN, VN, and (Ti, Nb)N film heterostructures by transmission electron microscopy. *J Cryst Growth* 135:309–317
- [17] Odén M, Ljungcrantz H, Hultman L (1997) Characterization of the induced plastic zone in a single crystal TiN (001) film by nanoindentation and transmission electron microscopy. *J Mater Res* 12:2134–2142
- [18] Li N, Yadav S, Liu XY, Wang J, Hoagland R, Mara N, Misra A (2015) Quantification of dislocation nucleation stress in TiN through high-resolution in situ indentation experiments and first principles calculations. *Sci Rep* 5:15813
- [19] Vahldiek F, Mersol S (1977) Slip and microhardness of IVa to VIa refractory materials. *J. Less Common Metals* 55:265–278
- [20] Li P, Howe J (2002) Dislocation reactions in ZrN. *Acta Mater* 50:4231–4239
- [21] Vinson K, Yu XX, De Leon N, Weinberger CR, Thompson GB (2016) Plasticity mechanisms in HfN at elevated and room temperature. *Sci Rep* 6:34571
- [22] Zhang R, Sheng S, Veprek S (2013) Origin of different plastic resistance of transition metal nitrides and carbides: Stiffer yet softer. *Scripta Mater* 68:913–916
- [23] Sangiovanni DG, Hultman L, Chirita V (2011) Super-toughening in B1 transition metal nitride alloys by increased valence electron concentration. *Acta Mater* 59:2121–2134
- [24] Li T, Morris J Jr, Nagasako N, Kuramoto S, Chrzan D (2007) Ideal engineering alloys. *Phys Rev Lett* 98:105503
- [25] Holleck H (1986) Material selection for hard coatings. *J Vac Sci Technol A* 4:2661–2669
- [26] Kresse G, Hafner J (1993) Ab initio molecular dynamics for liquid metals. *Phys Rev B* 47:558–561
- [27] Kresse G, Hafner J (1994) Ab initio molecular-dynamics simulation of the liquid-metal-amorphous-semiconductor transition in germanium. *Phys Rev B* 49:14251–14269
- [28] Kresse G, Furthmüller J (1996) Efficiency of ab-initio total energy calculations for metals and semiconductors using a plane-wave basis set. *Comput Mater Sci* 6:15–50
- [29] Kresse G, Furthmüller J (1996) Efficient iterative schemes for ab initio total-energy calculations using a plane-wave basis set. *Phys Rev B* 54:11169–11186
- [30] Blöchl PE (1994) Projector augmented-wave method. *Phys Rev B* 50:17953–17979
- [31] Kresse G, Joubert D (1999) From ultrasoft pseudopotentials to the projector augmented-wave method. *Phys Rev B* 59:1758–1775
- [32] Perdew JP, Burke K, Ernzerhof M (1996) Generalized gradient approximation made simple. *Phys Rev Lett* 77:3865
- [33] Abbena E, Salamon S, Gray A (2006) Modern differential geometry of curves and surfaces with mathematica. CRC Press, Cambridge
- [34] Tsukimoto S, Moriyama M, Murakami M (2004) Microstructure of amorphous tantalum nitride thin films. *Thin Solid Films* 460:222–226
- [35] Van Der Walt CM, Sole M (1967) On the plastic behaviour of crystals with the nacl-structure. *Acta Metall* 15:459–462
- [36] Tang W, Sanville E, Henkelman G (2009) A grid-based bader analysis algorithm without lattice bias. *J Phys Condens Matter* 21:084204
- [37] Jhi SH, Louie SG, Cohen ML, Ihm J (2001) Vacancy hardening and softening in transition metal carbides and nitrides. *Phys Rev Lett* 86:3348
- [38] Wu Z, Chen XJ, Struzhkin VV, Cohen RE (2005) Trends in elasticity and electronic structure of transition-metal nitrides and carbides from first principles. *Phys Rev B* 71:214103
- [39] Yu XX, Thompson GB, Weinberger CR (2015) Influence of carbon vacancy formation on the elastic constants and hardening mechanisms in transition metal carbides. *J Eur Ceram Soc* 35:95–103
- [40] Vinitskii I (1972) Relation between the properties of monocarbides of groups IV-V transition metals and their carbon content. *Powder Metall Metal Ceram* 11:488–493
- [41] Yu H, Guzewski M, Thompson GB, Weinberger CR (2016) A model for understanding the formation energies of nanolamellar phases in transition metal carbides and nitrides. *Model Simul Mat Sci Eng* 24:55004
- [42] Hirth JP, Lothe J (1982) Theory of dislocations. Wiley, New York
- [43] Carlson O, Smith J, Nafziger R (1986) The vanadium-nitrogen system: a review. *Metall Mater Trans A* 17:1647–1656
- [44] Brauer G (1960) Nitrides, carbonitrides and oxynitrides of niobium. *J Less Common Metals* 2:131–137
- [45] Pierson HO (1996) Handbook of refractory carbides and nitrides; properties characteristics, processing and applications. Noyes Publications, Westwood
- [46] Ryu S, Kang K, Cai W (2011) Predicting the dislocation nucleation rate as a function of temperature and stress. *J Mater Res* 26:2335–2354
- [47] Warner DH, Curtin W (2009) Origins and implications of temperature-dependent activation energy barriers for dislocation nucleation in face-centered cubic metals. *Acta Mater* 57:4267–4277
- [48] Kim C, Gottstein G, Grummon D (1994) Plastic flow and dislocation structures in tantalum carbide: deformation at low and intermediate homologous temperatures. *Acta Metall Mater* 42:2291–2301